

# Confirmation of Sensitivity for Detecting Anisotropy of Atmospheric Delay Using High-sensitivity Delay Measurement

Takaaki Jike<sup>1</sup>, Tomoaki Oyama<sup>1</sup>, Aya Yamauchi<sup>1</sup>, Hideki Ujihara<sup>2</sup>, Ryuichi Ichikawa<sup>3</sup>, Mamoru Sekido<sup>3</sup>, Hiroshi Munekane<sup>4</sup>, Basara Miyahara<sup>4</sup>, Tomokazu Kobayashi<sup>4</sup>, Hiroshi Takeuchi<sup>5</sup>, Hiroshi Imai<sup>6</sup>

**Abstract** To estimate the expected performance of atmospheric delay measurements obtained from the microwave radiometers currently under development, we use sensitive delay measurements from VERA K-band wideband geodetic VLBI observations, and we have estimated the anisotropy of atmospheric delays. The sky hemisphere was divided into a number of zones, and the zenith atmospheric delay modifications obtained within these zones were estimated. The results showed differences in the distribution of atmospheric delay residuals, normalized by the optical path length ratio of a few tens of picoseconds in each zone. With regard to anisotropy in the zenith angular direction, the closer to the zenith, the smaller the contribution of the atmospheric delay correction in the post-fit delay residual. Microwave radiometers are expected to separate atmospheric delay corrections from other error factors as fluctuations in optical path length with an accuracy of a few millimeters.

**Keywords** anisotropy of atmospheric delay

## 1 Introduction

We are involved in the development of next-generation microwave radiometers used in millimeter-wave spec-

troscopy to monitor atmospheric behavior with high resolution and precision (Grant-in-Aid for Scientific Research 21H04524, JSPS). By applying this radiometer to VLBI observations, it is possible to measure the atmospheric propagation delay of electromagnetic waves in the line-of-sight direction with high precision, and it is expected that the accuracy of measurement parameters will improve. On the other hand, VLBI observation data must also have a sensitivity commensurate with the measurement accuracy of this atmospheric delay. Since 2016, we have been conducting geodetic VLBI experiments in K-band, using the 8 Gbps recording device and performing highly accurate delay measurements [1]. We investigated the ability of these experiments to detect anisotropy along the azimuthal and zenithal angles of atmospheric delay. Such a validation was reported in Jike et al. (2019) [2] in a pilot study, which was further scrutinized using multiple data in the present study. As the results of that trial, anisotropy of atmospheric delay was detected with an accuracy of approximately a few tens of picoseconds. It is expected that this sensitivity will be utilized to verify the ability to measure atmospheric propagation delays using next-generation microwave radiometers.

## 2 Observation and Analysis

This section presents a list of observation sessions (Table 1) and the observation and analysis specifications (Table 2). The data we end up with are these post-fit delay residuals. The fitting parameters estimated to obtain the post-fit delay residuals are the modified station coordinates, polynomials of the modified clock offset,

1. National Astronomical Observatory of Japan
2. Ritumeikan University
3. National Institute of Information and Communication Technology
4. Geospatial Information Authority of Japan
5. Japan Aerospace Exploration Agency
6. Kagoshima University

and polynomials of the modified zenith atmosphere delay.

**Table 1** List of observing sessions.

Session	VERA Stations	Start Time (UT)	Duration
z19094k	Vm, Vr, Vo, Vs	2019y094d04:10	12 h
z21022k	Vr, Vo, Vs	2021y022d05:20	24 h
z21089k	Vm, Vr, Vo, Vs	2021y089d02:40	24 h

**Table 2** Specifications of observation and analysis.

Observation	Parameter
Diameter, Mount, Mirror	20 m, AZEL, Cassegrain
Beam Position	Single-beam, Ctr of Field Rotator
Frequency Range	21,459–23,507 MHz
DBBC Formatting Mode	1024 Msps-2bit-4stream, vdfif
Analysis	Parameter
Correlator Engine and Type	GICO3 FX
FFT	$2^{10}$ points/stream
Accumulation Freq.	1 Hz
Number of Corr. Unit	four units, one stream/unit
Analysis Tools	calc/msolv
EOP	EOP 20 C04
Apriori Zenith Atm. Delay	JMA objective analysis data
Mapping Function	Global Mapping Function
Iono. Delay Prediction	from slant TECU by CODE GIM

The post-fit delay residual normalized by optical path length  $R_z$  is expressed by the following equation.

$$R_z = R_{pf} / GMF_z,$$

where  $R_{pf}$  is a post-fit residual delay and  $GMF_z$  is the optical path length ratio due to the Global Mapping Function when the zenith angle at the subordinate station of the respective baseline is  $z$ . The root mean square (*RMS*) of  $R_z$  is shown in Table 3 at each of the independent baselines for each session. Overall, the *RMS*s were in the range of 15 to 30 picoseconds, but there was a clear tendency for the *RMS* to be larger for the baselines containing Vs than for the other baselines.

### 3 Spatio-temporal Distribution of $R_z$

Two zoning models are applied to identify the characteristics of the spatiotemporal distribution of  $R_z$ . The

**Table 3** *RMS* of  $R_z$ .

Session	Baseline (master–subordinate)	<i>RMS</i> of $R_z$ (ps)
z19094k	Vm–Vr	17.85
	Vm–Vo	20.11
	Vm–Vs	28.99
z21022k	Vr–Vo	17.44
	Vr–Vs	18.67
z21089k	Vm–Vr	15.20
	Vm–Vo	19.51
	Vm–Vs	22.81

first is divided into four zones in the azimuthal direction ( $-45^\circ$  to  $45^\circ$ ,  $45^\circ$  to  $135^\circ$ ,  $135^\circ$  to  $225^\circ$ , and  $225^\circ$  to  $315^\circ$ ) and the second into three zones by *GMF* (1 to 2, 2 to 3, and 3 to 5). As for time, both are divided into six-hour zones each. The distribution of  $R_z$  in the zone is represented in the box chart in Figures 1, 2, and 3.

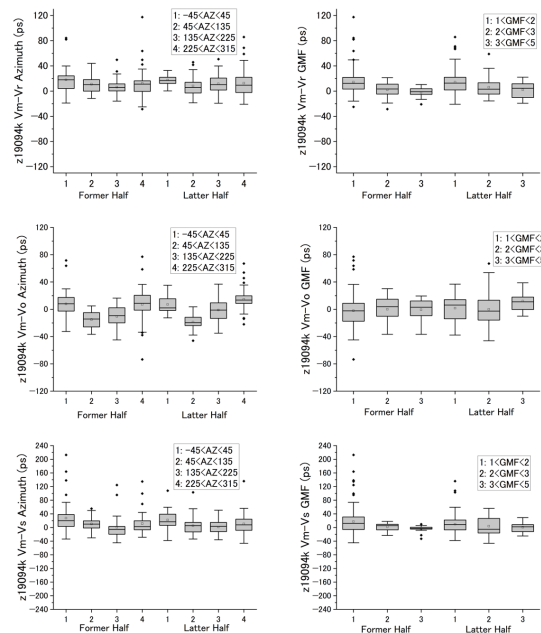


**Fig. 1** z19094k distributions of  $R_z$ .

Azimuthal anisotropy was observed in the distribution of  $R_z$  obtained from the six-hour post-fit delay residuals. There were several patterns of positive and negative divergence of the  $R_z$  distribution according to azimuth, with the magnitude of this anisotropy reaching up to 40 picoseconds. Furthermore, the pattern of azimuthal anisotropy changed with time, with a maximum variation of 20 picoseconds.

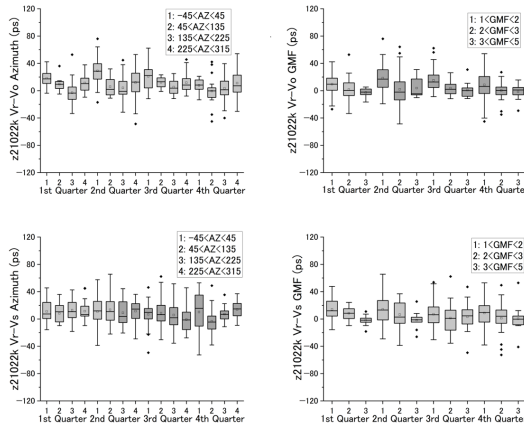


Fig. 2 z21022k distributions of  $R_z$ .

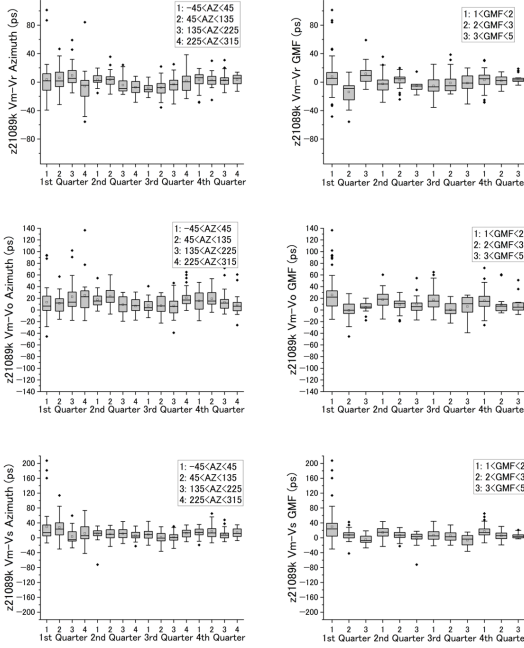


Fig. 3 z21089k distributions of  $R_z$ .

On the other hand, anisotropy along the axis of the optical path length ratio, the value of  $GMF$ , was also confirmed by the  $R_z$  calculated from six-hour post-fit delay residuals, with the magnitude of the spatio-temporal variation in this anisotropy reaching up to 20 picoseconds in maximum. The interquartile range of the distribution of the  $R_z$  tended to be larger in zones with smaller angles from the zenith, in which  $Vm-Vr$  and  $Vm-Vs$  in z19094k were particularly distinctive.

This shows that the effect of normalizing  $R_p f$  by  $GMF$  differs with respect to the zenith angle.

### 4 Considerations and Conclusion

To obtain the deviation of  $R_z$  ( $DEV$ ) in the azimuthal zone and  $GMF$  zone for each baseline of each session, the following equation is used, and the results are shown in Figures 4 and 5.

$$DEV_{(i,j)} = R_{z(i,j)} - \sum_{k=1}^n \left( \frac{R_{z(k)}}{n} \right),$$

where  $R_{z(i)}$  is the  $i$ -th  $R_z$  in  $j$ -th zone, and  $n$  is the total number of  $R_z$ . The graph represents the mean and standard deviation of the distribution of  $DEV_{(i,j)}$ .

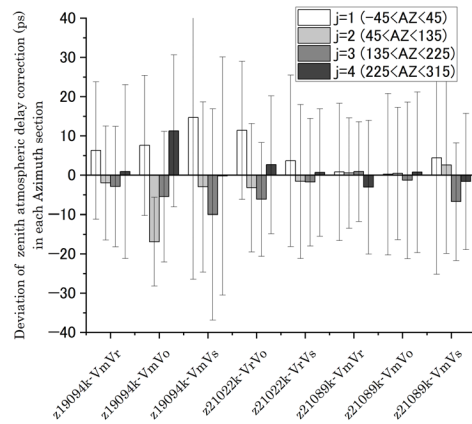


Fig. 4 Distribution of  $DEV$  on azimuthal angle.

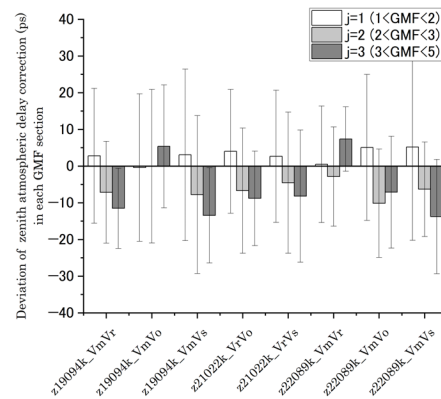


Fig. 5 Distribution of  $DEV$  on zenith angle.

A feature of the  $R_z$  deviation distribution in the azimuthal direction is that  $R_z$  in each azimuthal zone deviated by up to 18 picoseconds from the mean value obtained from all azimuthal directions at each session and at each baseline. Axial contrasting distributions were also identified for the majority of the  $R_z$  azimuthal anisotropy. This is thought to be a mixture of true atmospheric delay anisotropy and the effects of correction errors in the station coordinates, which are difficult to separate.

Next, the feature of the distribution of deviations in the zenith angle direction is that more than half of the  $R_z$  deviations were distributed in the positive range in the zones with the  $GMF$  optical path length ratios of 1 to 2. This suggests that apart from the deviation from the atmospheric propagation model, there is some error factor that changes the optical path length in the direction close to the zenith, including presumably an error in the vertical correction of the station coordinates, which is also difficult to separate from the atmospheric delay error.

The contribution ratio of the atmospheric delay correction to the delay residual for each azimuth and  $GMF$  zone is shown in Figures 6 and 7. The contribution rate for zone  $j$  ( $CR_j$ ) is expressed as follows,

$$CR_j = 1 - (\sigma R_{z(j)} / \sigma R_{pf(j)}),$$

where  $\sigma R_{z(j)}$  is the standard deviation of  $R_z$  in the  $j$ -th zone, and  $\sigma R_{pf(j)}$  is the standard deviation of  $R_{pf}$  in the  $j$ -th zone. If this contribution ratio is not constant, it indicates that the ratio of atmospheric delay to other error factors is variable in each zone.

From the results of Figure 6, the contribution ratios in each azimuthal zone are not constant and do not seem to be characteristic for a particular azimuthal angle. It is conceivable that the weather conditions, which vary from day to day and site to site, support this result.

Conversely, the contribution ratio in the  $GMF$  zone has a significant feature as shown in Figure 7. The contribution ratio in the same  $GMF$  zone is almost constant for different baselines within the same session, and it increases sequentially as the optical path length ratio increases, from about 0.2 for zone  $1 < GMF < 2$ , to about 0.6 for zone  $2 < GMF < 3$  and about 0.7 for zone  $3 < GMF$ . Furthermore, such a feature of the increase in the contribution ratio showed a similar trend in different sessions. This agrees with the fact that the size of the distribution of residuals has a term propor-

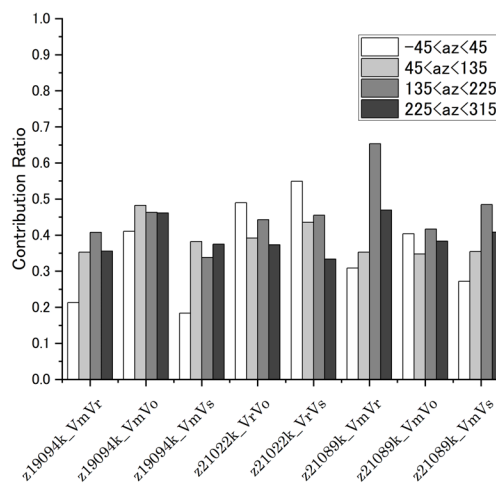


Fig. 6 Contribution ratio per azimuth zone.

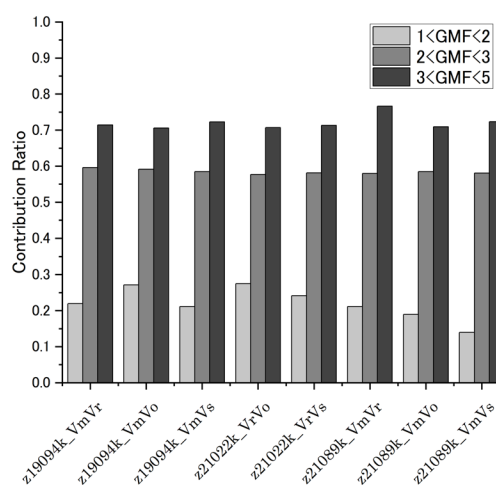


Fig. 7 Contribution ratio per  $GMF$  zone.

tional to the  $GMF$ . However, agreement tends to deteriorate in zones closer to the zenith. Although this is only speculation, structural deformation of the VERA antenna due to internal and external factors and changes in the electrical length of the antenna's transmission lines may also contribute to the error. The effects also seem to have a characteristic that tends to be more pronounced at smaller zenith angles. The distribution of post-fit delay residuals with respect to the optical path length ratio is shown for each session in Figure 8.

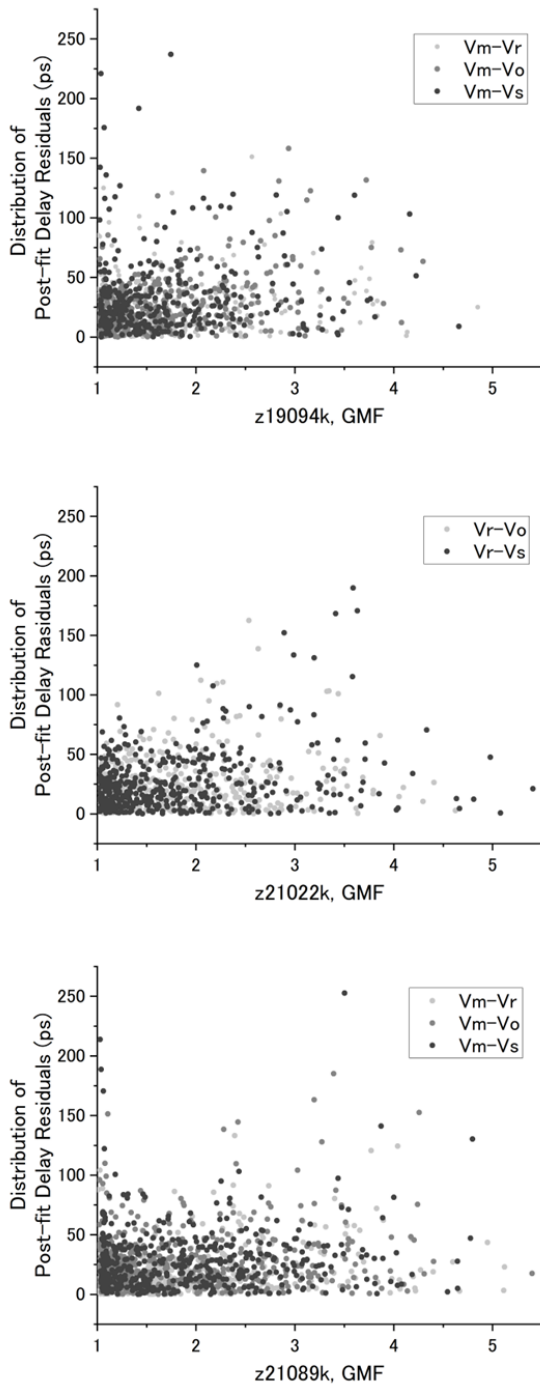


Fig. 8 Relationship  $R_{pf}$  to  $GMF$ .

The fact that  $CR$  is not constant for the  $GMF$  zone means that the distribution of post-fit delay residuals is not proportional, which is expected to be represented

in the graph, and indeed no such proportional relationship was identified, and characteristics indicating a link with other error factors are also unclear. It is assumed that this is due to the mingling of several elements of mis-estimation of the analysis parameters, and separating out this mis-estimated component is one of the important issues for us.

In order to separate errors due to mis-estimation of atmospheric delay from other errors, it is necessary to provide more accurate atmospheric delay parameters in the analysis. Our radiometer development studies are also expected to play an active role in separating atmospheric delay errors from other error components. For this purpose, it is desirable to detect changes in the optical path length of a few millimeters, which corresponds to delays of a few tens of picoseconds or less.

## References

1. T. Jike, "VERA Geodetic VLBI with a Newly Developed High-speed Sampler and Recorder", In D. Behrend, K. D. Baver, and K. L. Armstrong, editors, IVS 2016 General Meeting Proceedings, NASA/CP-2016-219016, pages 159–162, 2016.
2. T. Jike, T. Oyama, T. Nagayama, and A. Yamauchi, "Current Results of the VERA K/Q-band Fringe Survey: Performance of the 8-Gbps Recording System and its Effectiveness", In K. L. Armstrong, K. D. Baver, and D. Behrend, editors, IVS 2018 General Meeting Proceedings, NASA/CP-2019-219039, pages 66–70, 2019.